https://dx.doi.org/10.1016/j.jcsr.2017.07.003
This is the Pre-Published Version.

Static strength of high strength steel CHS X-joints under axial compression

Xiaoyi Lan [a], Tak-Ming Chan [a,*], Ben Young [b]

[a] Dept. of Civil and Environmental Engineering, The Hong Kong Polytechnic University, Hung Hom, Hong Kong, China

[b] Dept. of Civil Engineering, The University of Hong Kong, Pokfulam Road, Hong Kong, China

*tak-ming.chan@polyu.edu.hk

Abstract: This paper presents an investigation on static strength of high strength steel circular hollow section (CHS) X-joints subjected to axial compression in the braces failed by chord face plastification. Using validated finite element models, extensive numerical simulations were conducted considering a wide range of geometric parameters and chord preload ratios. The material properties of high strength steel with nominal yield stresses of 700, 900 and 1100 MPa were carefully incorporated in finite element models. The static strengths obtained from numerical analysis in this study and experimental tests in literature were compared with those calculated from nominal strength equations on which the design equations in Eurocode EN 1993-1-8 and CIDECT design guide are based. The comparison results show that the nominal strength equation adopted by CIDECT design guide is generally more accurate than that of EN 1993-1-8. The nominal strength prediction of CIDECT design guide without using reduction factors of joint strength is relatively accurate for CHS X-joints with nominal steel yield stresses ranging from 650 to 700 MPa. However, the nominal strength predictions of EN 1993-1-8 and CIDECT design guide generally become more unconservative with increasing steel yield stress. The nominal strength equations are not applicable for CHS X-joints with nominal steel yield stresses exceeding 700 MPa.

Keywords: Circular hollow section; High strength steel; Static strength; X-joints

Nomenclature

d	chord diameter	d_1	brace diameter
t	chord wall thickness	t_1	brace wall thickness
l	chord length	l_1	brace length
A_0	cross section area of chord member	τ	brace to chord wall thickness ratio (t_1/t)
β	brace to chord diameter ratio ($=d_1/d$)	2γ	chord diameter to wall thickness ratio ($=d/t$)
θ	angle between brace and chord members	n	chord preload ratio
f_y	yield stress	E	elastic modulus
COV	coefficient of variation	r_{si}	strength ratio ($=N_{ei}$ / N_{fi})
N_{ei}	joint strength calculated from nominal strength equations	N_{fi}	joint strength obtained from finite element analysis and tests

1. Introduction

High strength steel (HSS) with a nominal yield stress higher than 450 MPa has become readily available due to rapid development of steel production technology. The application of high strength steel can reduce structural self-weight and lower construction costs as well as carbon footprints by using less material. Thus, high strength steel is increasingly popular in construction industry as an economical and sustainable construction material.

© 2017. This manuscript version is made available under the CC-BY-NC-ND 4.0 license http://creativecommons.org/licenses/by-nc-nd/4.0/

Steel tubular joints are a critical part of onshore and offshore steel tubular structures. Comprehensive design rules for normal strength steel tubular joints with a nominal steel yield stress not exceeding 355 MPa are available in design codes and guides including Eurocode EN 1993-1-8 [1], CIDECT design guides [2, 3], ISO 14346 [4], IIW recommendations [5] and API RP 2A WSD [6]. However, there is limited design guidance for HSS tubular joints. For steel tubular joints using steel grades greater than S355 and up to S460, an additional reduction factor of joint strength of 0.9, combined with the limitation on yield stress (f_y) to 0.8 of ultimate stress ($0.8f_u$), is specified in CIDECT design guides [2, 3]. Similarly, EN 1993-1-8 [1] stipulates a reduction factor of 0.9 for steel tubular joints in steel grades greater than S355 and up to S460. EN 1993-1-12 [7] further extends the use of steel up to grade S700 and imposes a reduction factor of 0.8 for steel tubular joints using steel grades greater than S460 and up to S700. These restrictions in Eurocode [1, 7] and CIDECT design guides [2, 3] for HSS tubular joints are stipulated due to relatively large deformation observed in chord face plastification failure, lower deformation capacity of steel with yield stresses exceeding 355 MPa, and required sufficient joint ductility for punching shear and effective width failure [8]. Such punitive provisions are based on limited research on HSS tubular joints.

Kurobane [9] conducted experimental investigation on circular hollow section (CHS) gap K-joints made of S460 steel. It is found that the joint strength is 18% lower than that of corresponding S235 joints in relative terms after taking account for the increased yield stress. Liu and Wardenier [10] carried out numerical study on rectangular hollow section (RHS) gap K-joints using S460 steel and found that the reduction of joint strength varies from 10 to 16% compared with corresponding S235 joints. Fleischer et al. [11] conducted finite element analysis on the reduction factor of the static strength of CHS X-joints made of S460 and S690 steel compared with corresponding S355 joints. It is found that the reduction factors are marginally higher than 0.9 for S460 joints and higher than 0.8 for S690 joints. Puthli et al. [12] carried out experimental tests on CHS right angle X-joints using steel grades up to S770 without considering chord axial stress effect. It is found that the test strength generally exceeds the design strength in EN 1993-1-8 [1] without using the reduction factors. Becque and Wilkinson [13] conducted tests on RHS T- and X-joints made of C450 steel with a nominal yield stress of 450 MPa. It is found that the test strength is higher than the nominal strength converted from the design strength in CIDECT design guide [2]. It is without imposing the reduction factor and limitation on the yield stress for the joints failed in ductile modes (i.e. chord face plastification and side wall buckling), provided the geometric limits in CIDECT provisions are satisfied. However, the test results justify the introduction of the reduction factor and limitation on yield stress for the joints failed by fracture, in particular, punching shear and effective width failures. Mohan et al. [14-15] carried out numerical investigation on RHS T-, X-, K- and N-joints using C450 steel. The numerical strength is found to be generally higher than the design strength without the reduction factor and limitation on yield stress in CIDECT design guide [2]. Cheng et al. [16] proposed a design methodology for equal-width RHS X-joints using steel grades up to C450 failed by chord side wall buckling. Lee et al. [17] conducted experimental tests and numerical analysis on CHS X-joints made of HSA800 steel with measured yield stresses up to 800 MPa without chord preload. It is found that the joint strength exceeds the design strength in EN 1993-1-8 [1] without using the reduction factor. However, research on high strength steel tubular joints with steel yield stresses higher than 700 MPa remains limited.

A numerical study on the static strength of CHS X-joints with nominal steel yield stresses of 700, 900 and 1100 MPa under axial compression was conducted. The numerical study covered a wide range of geometric parameters and chord preload ratios. The static strength obtained from numerical analysis and experimental tests available in literature was compared with that calculated from nominal strength equations on which the design equations in EN 1993-1-8 [1] and CIDECT design guide [3] are based. The

suitability of current design rules for high strength steel CHS X-joints failed by chord face plastification was evaluated.

2. Finite element model

The finite element (FE) program ABAQUS [18] was used to carry out the numerical analysis. Test results of CHS X-joints made of S355, S690 and S770 steel [12] and HSA800 steel [17] subjected to axial compression in the braces were used to validate the FE models. Table 1 shows the parameters of CHS X-joints, namely chord diameter (d), chord wall thickness (t), brace diameter (d_1), brace wall thickness (t_1), the ratio (β) of brace diameter (d_1) to chord diameter (d), and the ratio (2γ) of chord diameter (d) to chord wall thickness (t). The angle (θ) between brace and chord members of specimens is 90°. Other parameters not listed in Table 1 are detailed in Puthli et al. [12] and Lee et al. [17]. It should be noted that the static strength of CHS X-joints is determined by the peak load or 3% indentation at the chord crown (i.e. indentation limit up to 3%d) in load-indentation curves proposed by Lu et al. [19]. The indentation refers to the distance between the original position of the chord crown and that when loads in the brace are applied. The indentation in this study was taken as the largest indentation value at the crown positions of CHS X-joints. If the indentation at the peak load is smaller than 3%d, then the peak load is considered to be the joint strength. If the indentation at the peak load is larger than 3%d, then the load at the indentation of 3%d is considered to be the joint strength.

2.1. Material properties

Puthli et al. [12] and Lee et al. [17] only reported the yield stress (f_y) and ultimate stress (f_u) of steel grades S355 (specimen R47), S690 (specimens R32 and R33), S770 (specimens R69, R71 and R75) and HSA 800 (specimens X90-650-0.75-16 and X90-650-0.62-26), as shown in Table 1. However, the stress-strain curves for the steel materials of specimens were not reported [12, 17]. Therefore, a bi-linear stress-strain curve for all steel grades was adopted, and the values of elastic modulus (E), and ultimate strain (ε_u) corresponding to ultimate stress are 210 GPa and 10%, respectively, in accordance with Fleischer et al. [11] and Puthli et al. [12]. The Poisson's ratio (v) equals to 0.3. The true stress-strain curve was input in FE models after converting the engineering stress-strain curve using the following equations [20]:

$$\varepsilon_T = \ln(1+\varepsilon) \tag{1}$$

$$\sigma_T = \sigma(1+\varepsilon) \tag{2}$$

where ε_T and ε are true and engineering strain, respectively, and σ_T and σ are true and engineering stress, respectively. The same material properties for the chord, brace and weld were adopted [11, 12]. The von Mises yield surface criterion and isotropic strain hardening rules were used.

2.2. Loading and boundary conditions

All degrees of freedom at the end of the two braces were restricted, except for the brace axial displacement, and the two chord ends were free to translate and rotate. The loads were applied in increments by using the "Static" method in the ABAQUS library. The nonlinear geometric parameter

(*NLGEOM) was used to consider the effect of large displacement in FE analysis.

2.3. Element type and weld modelling

The effect of element type and weld modelling on the prediction of the structural behavior and static strength of CHS X-joints is investigated in this subsection. CHS X-joints were modelled using shell element without modelling the weld and solid element with weld modelling for comparison. Specimens R69, R71 and R75 listed in Table 1 were selected for the comparison study.

2.3.1. Shell element without weld modelling

A shell element S4R (four-node quadrilateral shell element) was adopted to model brace and chord members without modelling the weld. Five integration points through the shell element thickness was employed. The suitable mesh size was determined by a mesh convergence study. A coarse mesh size was used for members outside the joint zone while a finer mesh size was employed in the joint zone. Table 2 shows the comparison of FE strength (N_{FE}) using different mesh sizes with test strength (N_{Test}) of specimen R69 [12]. It is found that mesh sizes of 5 and 10 mm for the joint zone and members outside joint zone are suitable. Fig.1(a) shows the corresponding mesh layout for specimen R69. A similar mesh convergence study was conducted to determine the suitable mesh size for other specimens in Table 1, and the adopted mesh sizes are shown in Table 3.

2.3.2. Solid element with welding modelling

C3D8R (eight-node solid element) were selected in modelling the brace and chord members. C3D6 (wedge solid element) was adopted to model the weld. The measured dimensions of welds detailed in Puthli et al. [12] were modelled. The weld was tied to the surfaces of brace and chord members using “tie” function in ABAQUS. The weld was chosen as the slave surface, and the brace and chord members were selected as the master surface. Four layers of solid elements were used through the tube wall thickness for thick-walled tubular members ($2\gamma \leq 20$), while two layers of solid elements were employed for thin-walled tubular members ($2\gamma \geq 20$) [21]. A similar mesh convergence study as described in Section 2.3.1 was conducted for FE models using solid element. Table 2 shows the result of mesh convergence study for specimen R69 using solid element. It is found that the mesh sizes of 8 and 16 mm for the joint zone and members outside the joint zone are suitable. The suitable mesh size for the weld is 3 mm. Fig. 1(b) and Fig. 1(c) show the corresponding mesh layouts. The suitable mesh sizes of solid element adopted for specimens R69, R71 and R75 are summarized in Table 3.

2.3.3. Comparison result

Fig. 2(a) shows the comparison of the load-indentation curves of specimens R69, R71 and R75 using shell and solid elements with those obtained from tests. It is shown that FE models using both shell and solid elements can produce reasonably accurate prediction of load-indentation curves. It should be noted that the discrepancy in the load-indentation curves is possibly due to the adopted simplified bi-linear material curve in FE simulations. Fig. 3 further compares the failure mode of specimen R75 observed in test and that obtained from finite element analysis (FEA). The areas in red on the chord face at the

brace-chord intersection in Fig. 3 (b) and Fig. 3(c) became plastic. It is shown that the adopted FE models can produce close prediction of the failure mode (i.e. chord face plastification) of the tested specimen. Table 3 shows the comparison of test strength (N_{Test}) of specimens R69, R71 and R75 with corresponding numerical strength (N_{FE}) using solid and shell elements. It is shown that maximum discrepancy in the prediction of joint strength using shell and solid elements is 5% of the test strength (specimen R71). The comparison study shows that the effects of weld modelling and element type on the structural behavior and static strength of CHS X-joints under brace axial compression are insignificant. Thus, the shell element S4R was used to model other specimens in Table 1 without modelling the weld.

2.5. Validation

The comparison of FE strength (N_{FE}) with test strength (N_{Test}) is summarized in Table 3. It is shown that static strengths of all eight specimens are well predicted with a maximum discrepancy of 8% of the test strength. The mean value of N_{FE}/N_{Test} ratio is 1.02 with corresponding coefficient of variation (COV) of 0.051. The validation study shows that the adopted FE models using shell and solid elements can produce reasonably accurate predictions of the failure mode, load-indentation curve and static strength of CHS X-joints. It is noted that the computational cost of FE models using solid element is relatively high compared with FE models using shell element as higher mesh refinement through the thickness of brace and chord members is needed to obtain sufficient accuracy. Thus, the validated FE model using shell element S4R without modelling weld will be used in the subsequent numerical investigation.

3. Parametric study

3.1. General

An extensive numerical parametric study on CHS X-joints made of S700, S900 and S1100 steel was conducted. The joint parameters are shown in Table 4 including chord diameter (d), chord wall thickness (t), brace diameter (d_1), brace wall thickness (t_1), angle between brace and chord members (θ), chord preload ratio (n), the ratio (τ) of brace wall thickness (t_1) to chord wall thickness (t), the ratio (2γ) of chord diameter (d) to chord wall thickness (t), and the ratio (β) of brace diameter (d_1) to chord diameter (d). The chord preload ratio (n) equals to the ratio of compressive chord preload (N_p) to chord yield load ($A_0 f_y$). The joint configuration and notations of CHS X-joints in the parametric study are shown in Fig. 4. The specimens were carefully designed to cover a wide range of parameters, including β ($=d_1/d$), 2γ ($=d/t$), τ ($=t_1/t$), θ, and n. The joint parameter ranges are $0.2\leq\beta\leq1.0$, $10\leq2\gamma\leq50$, $0.5\leq\tau\leq1.0$, $30°\leq\theta\leq90°$ and $0\leq n\leq0.8$. The length of chord members (l) is equal to 6 times of chord diameter ($6d$) to ensure that the stresses at the brace-chord intersection are not influenced by the ends of the chord. The length of brace members (l_1) is equal to 3 times of brace diameter ($3d_1$), in order to prevent occurrence of overall buckling of brace members, which can not reveal the true static strength of tubular joints. Specimen label of each joint consists of one letter and one number. The letter (H, V or S) denotes the steel grade (S700, S900 or S1100). The number represents the corresponding joint geometric parameters and chord preload ratios, as shown in Table 4. For example, H1 denotes CHS X-joints made of S700 steel. The joint geometric parameters and chord preload ratio (n) of H1 are listed in Table 4.

The material properties of S700, S900 and S1100 steel in Ma et al. [22] were used in the FE simulation. Table 5 shows the material parameters including elastic modulus (E), stress at plastic strain of 0.01% ($\sigma_{0.01}$),

0.2% yield stress ($\sigma_{0.2}$), ultimate stress (σ_u) and ultimate strain at ultimate stress (ε_u). Fig. 5 shows the adopted stress-strain curves. A shell element S4R was adopted. The mesh convergence study shows that the mesh size of 4 mm for CHS X-joints in Table 4 is suitable. For CHS X-joints without chord preload, all degrees of freedom at the end of braces were restricted, except for the brace axial displacement, and the two chord ends were free to translate and rotate. The axial compression was applied by displacement at the brace end. For CHS X-joints with chord preload, all degrees of freedom at the brace ends and chord ends were restricted, except for the axial displacement at the two brace ends and chord axial displacement at one end. The boundary conditions at the two chord ends were firstly set and then the chord preload was applied. Subsequently, the boundary conditions at the two brace ends were set and the brace ends were loaded by displacement.

3.2. Numerical results

The load-indentation curves of CHS X-joints made of S700, S900 and S1100 steel obtained from finite element analysis are shown in Figs. 6-8, respectively. The load refers to the axial compression applied at the brace end and the indentation denotes the largest indentation at the crown position (see Fig. 4). The indentation limit of 3%d is denoted by the solid line in Figs. 6-8. The numerical joint strengths (N_{FE}) are summarized in Tables 6-8. The failure mode of CHS X-joints analyzed is chord face plastification. It should be noted that the failure modes of brace local buckling and chord punching shear of CHS X-joints were not investigated in this study. It is because brace local buckling can be prevented by using Class 1 or 2 cross-sections for the brace member and chord punching shear is brittle failure which cannot be well simulated by the adopted FE models herein. Figs. 6-8 show that the static strength of CHS X-joints made of high strength steel decreases with decreasing β ($=d_1/d$), and with increasing 2γ ($=d/t$), θ, and n ($=N_p/A_0f_y$). The effect of τ ($=t_1/t$) on the joint strength is insignificant. These observations concur with test and numerical results [12, 17] in which the effect of n ratio was not investigated. It is noted that the effect of these parameters on static strength of high strength steel CHS X-joints is similar to that of corresponding normal strength steel joints, as indicated in design codes and guides [1-6].

4. Comparison and evaluation of design rules

4.1. General

The applicability of design rules in EN 1993-1-8 [1] and CIDECT design guide [3] for CHS X-joints with steel yield stresses higher than 700 MPa and up to 1200 MPa was assessed. It is noted that the design rules for normal strength steel CHS X-joints in CIDECT design guide [3], ISO 14346 [4] and IIW recommendations [5] are the same. API RP 2A WSD [6] adopts a different deformation limit, i.e. Yura displacement limit of $60d_1f_y/E$ instead of the deformation limit of 3%d [23]. Thus, it is not included in the comparison study to allow consistent comparison. In this study, the nominal strength of CHS X-joints failed by chord face plastification was calculated from nominal strength equations on which the design equations in EN 1993-1-8 [1] and CIDECT design guide [3] are based. The nominal strength predictions were compared with the numerical strengths obtained in this study and test strengths in literature [12, 17].

4.2. Comparison of nominal strengths

The design equations for normal strength steel CHS X-joints under brace and chord axial compression failed by chord face plastification in EN 1993-1-8 [1] and CIDECT design guide [3] are as follows:

$$N_{EC,Rd} = \frac{k_p f_y t^2}{\sin\theta} \frac{5.2}{(1-0.81\beta)} / \gamma_{M5} \quad \text{(EN 1993-1-8) [1]} \quad (3)$$

$$k_p = 1 - 0.3n(1+n) \qquad n = \frac{N_p}{A_0 f_y} \quad (4)$$

$$N_{CIDECT,Rd} = 2.6\left(\frac{1+\beta}{1-0.7\beta}\right)\gamma^{0.15} Q_f \frac{f_y t^2}{\sin\theta} \quad \text{(CIDECT design guide) [3]} \quad (5)$$

$$Q_f = (1-|n|)^{0.45-0.25\beta} \quad (6)$$

where f_y is the steel yield stress of the chord member, t is the chord wall thickness, β is the ratio of brace diameter (d_1) to chord diameter (d), and γ is the ratio of chord diameter (d) to twice chord wall thickness (t), θ is the angle between brace and chord members, γ_{M5} is the partial safety factor which equals to 1.0, N_p is the compressive chord preload, A_0 is the cross-section area of the chord, n is the chord preload ratio, k_p and Q_f are the parameters that account for the effect of compressive chord longitudinal stresses. Table 9 shows the validity ranges of these design equations and parameter ranges of the conducted numerical analysis.

The design equations in EN 1993-1-8 [1] are based on the modified Togo formula and deformation limit was not included [24]. Details of the development of the design equations in EN 1993-1-8 [1] are introduced in Wardenier [24]. The nominal strength equation on which the design equation (Eq. (3)) is based is as follow:

$$N_{EC} = \frac{k_p f_y t^2}{\sin\theta} \frac{7.46}{1-0.812\beta} (2\gamma)^{-0.05} \left(\frac{f_y}{f_u}\right)^{-0.173} \quad (7)$$

It is noted that Eq. (7) is relatively insensitive to the variations of 2γ ($=d/t$) and the yield ratio of steel yield stress (f_y) to ultimate stress (f_u) of chord members. Thus, 2γ=40 and f_y/f_u =0.66 were substituted in Eq. (7), and it is simplified as follow:

$$N_{EC} = \frac{k_p f_y t^2}{\sin\theta} \frac{6.67}{1-0.812\beta} \quad (8)$$

It should be noted that Eq. (7) is proposed based on the test results of CHS X-joints with nominal steel yield stress not exceeding 335 MPa. Thus, it is reasonable to assume that the yield ratio (f_y/f_u) of normal strength steel equals to 0.66 to simplify the function of the yield ratio. However, the yield ratio of high strength steel is higher and gets closer to 1.0. It is therefore desirable to examine the accuracy of Eq. (8) for high strength steel CHS X-joints because of the increased yield ratio. It is noted that a safety factor of roughly 1.28 has been built into the design equation (Eq. (3)) in EN 1993-1-8 [1] compared with the nominal strength equation (Eq. (8)).

The design equations in CIDECT design guide [3], on the other hand, are based on the analysis by van der Vegte et al. [25] and the 3% indentation limit is adopted in the determination of joint strength. The nominal strength equation based on numerical and test results for CHS X-joints made of normal strength steel is as follow [25]:

$$N_{CIDECT} = 3.16\left(\frac{1+\beta}{1-0.7\beta}\right)\gamma^{0.15} Q_f \frac{f_y t^2}{\sin\theta} \quad (9)$$

It is noted that an implicit safety factor of roughly 1.22 has been incorporated in Eq. (5) compared with the corresponding nominal strength equation (Eq. (9)).

To allow a direct and objective comparison, nominal strengths (N_{EC} and N_{CIDECT}) were calculated using Eqs. (8-9) and compared with the joint strength obtained from numerical analysis (N_{FE}) and experimental tests (N_{Test}). Tables 6-8 and Table 10 summarize the ratios of nominal strengths N_{ei} (i.e. N_{EC} and N_{CIDECT}) to numerical and test strengths N_{fi} (i.e. N_{FE} and N_{Test}). Fig. 9 shows the comparison of numerical and test strengths with nominal strength predictions. It should be noted that the specimens listed in Table 10 under brace axial compression failed by chord face plastification.

4.3. Evaluation of design rules

The strength ratio (r_{si}) of nominal strengths (N_{ei}) to numerical and test strengths (N_{fi}) was defined to evaluate the design rules of EN 1993-1-8 [1] and CIDECT design guide [3]. Table 6 shows that the mean values of N_{EC} / N_{FE} and N_{CIDECT} / N_{FE} ratios for steel grade S700 are 1.08 and 1.00 with corresponding coefficients of variation (COV) of 0.09 and 0.07. It indicates that the nominal strength predictions are relatively accurate in general. Table 7 shows that the mean values of N_{EC} / N_{FE} and N_{CIDECT} / N_{FE} ratios for steel grade S900 are 1.15 and 1.07 with corresponding COV of 0.10 and 0.10. It is shown that the nominal strength equations generally overpredict the numerical strengths. Table 8 shows that the mean values of N_{EC} / N_{FE} and N_{CIDECT} / N_{FE} ratios for steel grade S1100 are 1.32 and 1.23 with corresponding COV of 0.11 and 0.12. It therefore indicates that the nominal strength equations are unconservative for steel grade S1100. Table 10 shows that the mean values of N_{EC} / N_{Test} and N_{CIDECT} / N_{Test} ratios for CHS X-joints with steel yield stresses ranging from 727 to 904 MPa in tests [12, 17] are 1.28 and 1.17 with corresponding COV of 0.08 and 0.07. It is shown that the nominal strength predictions of CIDECT design guide [3] are relatively accurate for steel grades of S690 and HSA800, but become more unconservative for higher steel grade of S770. Nominal strength predictions of EN 1993-1-8 [1] are generally unconservative for all steel grades S690, S770 and HSA800. Fig. 9 shows that the strength ratio generally increases with increasing steel yield stress.

An error analysis was conducted to further evaluate the accuracy of the nominal strength equations. Table 11 shows the result of error analysis of the strength ratio (r_{si}= N_{ei}/N_{fi}, i=1 to N) for the nominal equations. In this study, numerical results of 90 CHS X-joints and test data of 12 CHS X-joints [12, 17] were combined for the statistical analysis. Thus, the total number (N) of analysed joints equals to 102. The relative error (e_i), the average relative error (e), and relative standard deviation (s) are defined as follows:

$$e_i = \frac{N_{fi} - N_{ei}}{N_{fi}} (i = 1, 2, 3, ..., N) \tag{10}$$

$$e = \frac{\sum_{i=1}^{N} |e_i|}{N} \tag{11}$$

$$s = \sqrt{\frac{\sum_{i=1}^{N} |e_i|^2}{N-1}} \tag{12}$$

Table 11 shows that the nominal strength equation adopted by CIDECT design guide [3] can produce more

accurate strength predictions with mean value of 1.11 and lower values of COV, e and s of 0.13, 13.5% and 18.2% than that in EN 1993-1-8 [1] with mean value, COV, e and s of 1.19, 0.13, 20.7% and 24.9%. In general, the following points can be observed from the comparison study:

The effect of β, γ and n ratios on the strength ratio (r_{si}) is significant. The strength ratio generally increases with decreasing ratios of β and n and with increasing γ ratio. It is noted that the functions of β, γ and n ratios in the nominal strength equations (Eqs. (8-9)) are obtained from regression analysis based on test and numerical results of normal strength steel CHS X-joints [24, 25]. The τ and θ ratios have minor effect on the strength ratio. It is therefore necessary to further examine the applicability of the functions of β, γ and n ratios for high strength steel CHS X-joints in future research.

The steel grade has significant effect on the strength ratio. The strength ratio generally increases with increasing steel yield stress. It is noted that the function of the steel yield ratio (f_y/f_u) in the nominal strength equations for normal strength steel CHS X-joints equals to specific values for simplification as discussed in Section 4.2. However, the yield ratio of high strength steel is higher than that of normal strength steel. It is desirable to investigate whether such simplification is reasonable for high strength steel CHS X-joints in future study. Comprehensive evaluation of the effect of the increased yield ratio has to involve analysis of larger database of test and numerical results.

The nominal strength equation adopted by CIDECT design guide [3] is generally more accurate than that of EN 1993-1-8 [1]. The nominal strength predictions of CIDECT design guide [3] are relatively accurate for CHS X-joints with nominal steel yield stresses ranging from 650 to 700 MPa. It therefore indicates that the reduction factor of joint strength of 0.8 stipulated in EN 1993-1-12 [7] may not be necessary. However, the nominal strength equations adopted by EN 1993-1-8 [1] and CIDECT design guide [3], in general, increasingly overpredict the static strength of CHS X-joints with higher steel yield stresses. The nominal strength predictions of EN 1993-1-8 [1] and CIDECT design guide [3] are unconservative for CHS X-joints with nominal steel yield stresses exceeding 700 MPa. It therefore indicates that the nominal strength equations are not applicable for CHS X-joints with nominal steel yield stresses higher than 700 MPa.

5. Conclusions

The static strength of high strength steel CHS X-joints with nominal steel yield stresses ranging from 650 to 1100 MPa subjected to axial compression in braces was investigated. The failure mode of CHS X-joints analysed is chord face plastification. An extensive numerical analysis covering a wide range of geometric parameters and chord preload ratios was conducted. The strength ratio of joint strengths calculated from nominal strength equations on which the design equations in EN 1993-1-8 and CIDECT design guide are based to those obtained from numerical simulations and experimental tests in literature was analysed. The conclusions are summarized as follows:

(1) The strength ratio generally increases with decreasing β and n ratios and with increasing γ ratio, and the effect of τ and θ ratios on the strength ratio is minor. The strength ratio generally increases with increasing steel yield stress.
(2) The nominal strength equation adopted by CIDECT design guide is generally more accurate than that of EN 1993-1-8. The nominal strength predictions of CIDECT design guide without using the reduction factor of joint strength are relatively accurate for CHS X-joints with nominal steel yield stresses ranging from 650 to 700 MPa.

(3) The nominal strength predictions of EN 1993-1-8 and CIDECT design guide generally become increasingly unconservative with increasing steel yield stress. The nominal strength equations adopted by EN 1993-1-8 and CIDECT design guide are not applicable for CHS X-joints with nominal steel yield stresses exceeding 700 MPa.

6. Acknowledgements

The authors appreciate the support from the Hong Kong Branch of the Chinese National Engineering Research Centre for Steel Construction. The first author is also grateful for the support given by the Research Grants Council of Hong Kong for the Hong Kong PhD Fellowship Scheme.

References

[1] Eurocode 3 (EC3), Design of steel structures-Part 1-8: Design of joints. European Committee for Standardization, EN 1993-1-8, CEN. Brussels, 2005.

[2] Packer J.A., Wardenier J., Zhao X.L., van der Vegte A., Kurobane Y. Design guide for rectangular hollow section (RHS) joints under predominantly static loading. CIDECT, Verlag TUV Rheinland. Cologne, Germany, 2009.

[3] Wardenier J., Kurobane Y., Packer J.A., van der Vegte A., Zhao X.L. Design guide for circular hollow section (CHS) joints under predominantly static loading. CIDECT, Verlag TUV Rheinland. Cologne, Germany, 2008.

[4] ISO. Static design procedure for welded hollow-section joints-Recommendations. ISO/FDIS 14346: 2012(E), Geneva.

[5] International Institute of Welding (IIW). XV-1439-13: Static design procedure for welded hollow section joints-Recommendations. Paris, 2013.

[6] American Petroleum Institute (API), Recommended Practice for Planning, Designing and Constructing Fixed Offshore Platforms-Working Stress Design. API Recommended Practice 2A WSD (RP 2A WSD), 22nd Ed., Washington, 2014.

[7] EN 1993-1-12. Eurocode 3: Design of steel structures-Part 1-12: additional rules for the extension of EN 1993 up to steel grades S700, European Committee for Standardization, EN 1993-1-12, CEN. Brussels, 2007.

[8] Zhao X.L., Wardenier J., Packer J.A., van der Vegte G.J. New IIW (2008) static design recommendations for hollow section joints, Tubular Structures XII, 2009, 261-269, Shanghai.

[9] Kurobane Y. New development and practices in tubular joint design, IIW Doc. XV-448-81 and IIW Doc. XIII-1004-81, 1981.

[10] Liu D.K., Wardenier J. Effect of the yield strength on the static strength of uniplanar K-joints in RHS (steel grade S460, S355 and S235), IIW Doc. XV-E-04-293, 2004.

[11] Fleischer O., Herion S., Puthli R. Numerical investigation on the static behaviour of CHS X joints made of high strength steels, Tubular Structures XII, 2008, 597-605, Shanghai.

[12] Puthli R., Bucak O., Herion S., Fleischer O., Fischl A., Josat O. Adaptation and extension of the valid design formulae for joints made of high-strength steels up to S690 for cold-formed and hot-rolled sections, CIDECT report 5BT-7/10 (draft final report), Germany, 2011.

[13] Becque J., Wilkinson T. The capacity of grade C450 cold-formed rectangular hollow section T and X connections: An experimental investigation, J. Const. Steel Res 133 (2017) 345-359.

[14] Mohan M., Wilkinson T. FEA of T & X joints in Grade C450 steel, Tubular Structures XIV, 2012, 185-194, London.
[15] Mohan M., Wilkinson T. Finite element simulations of 450 grade cold-formed K and N joints, Tubular Structures XV, 2015, 449-456, Brazil.
[16] Cheng S.S., Becque J. A design methodology for side wall failure of RHS truss X-joints accounting for compressive chord pre-load, Eng. Struct. 126 (2016) 689-702.
[17] Lee C.H., Kim S.H., Chung D.H., Kim D.K., Kim J.W. Experimental and numerical study of cold-formed high-strength steel CHS X-joints, J. Struct. Eng. 143(8) (2017) 04017077.
[18] Abaqus/Standard. Version 6.13-1. USA: K. a. S. Hibbit; 2013.
[19] Lu L.H., de Winkel G.D., Yu Y., Wardenier J. Deformation limit for the ultimate strength of hollow section joints, Tubular Structures VI, 1994, 341-347, Melbourne.
[20] Boresi A.P., Schmidt R.J. Advanced mechanics of materials. 6th ed. John Wiley and Sons; 2003.
[21] Choo Y.S., Qian X.D., Liew J.Y.R., Wardenier J. Static strength of thick-walled CHS X-joints-Part I. New approach in strength definition, J. Const. Steel Res 59(10) (2013) 1201-1228.
[22] Ma J.L., Chan T.M., Young B. Material properties and residual stresses of cold-formed high strength steel hollow sections. J. Const. Steel Res 109 (2015) 152-165.
[23] Pecknold D., Marshall P., Bucknell J. New API RP2A tubular joint strength design provisions, J. Energ. Resour. 129 (2007) 177-189.
[24] Wardenier J. Hollow section joints, Delft University Press, The Netherlands, 1982.
[25] van der Vegte G.J., Wardenier J., Zhao X.L., Packer J.A. Evaluation of new CHS strength formulae to design strengths, Tubular Structures XII, 2009, 313-322, London.

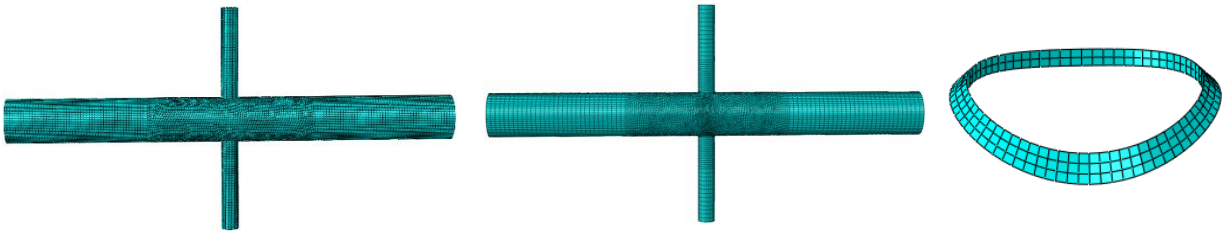

(a) Chord and brace using S4R (b) Chord and brace using C3D8R (c) Weld using C3D6

Fig. 1. Mesh layout of CHS X-joints.

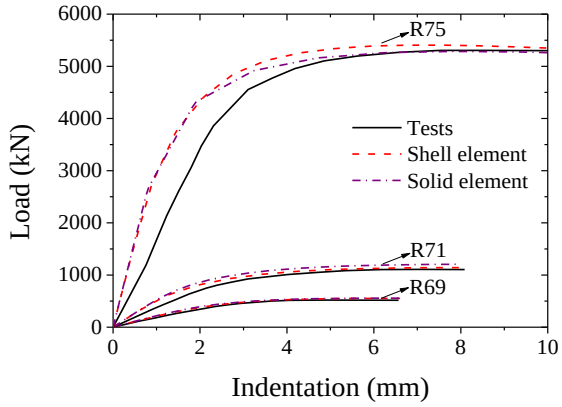

(a) Using shell and solid elements

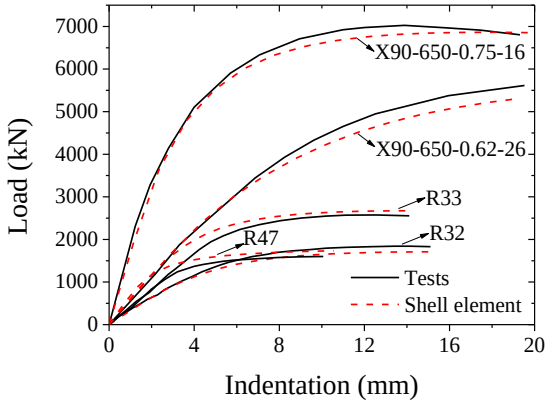

(b) Using shell element

Fig. 2. Comparison of load-indentation curve.

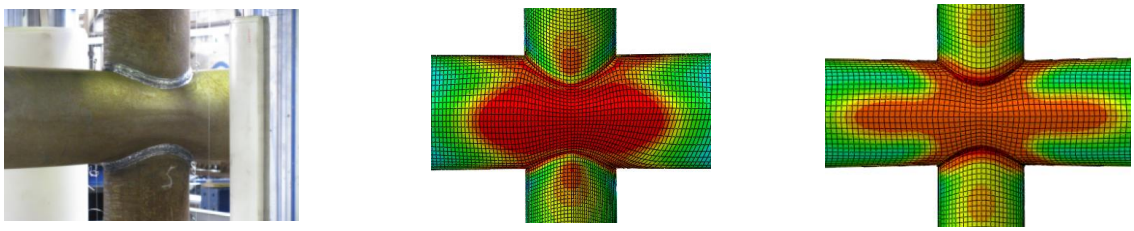

(a) Test observation (b) FEA using shell element (c) FEA using solid element

Fig. 3. Comparison of failure mode.

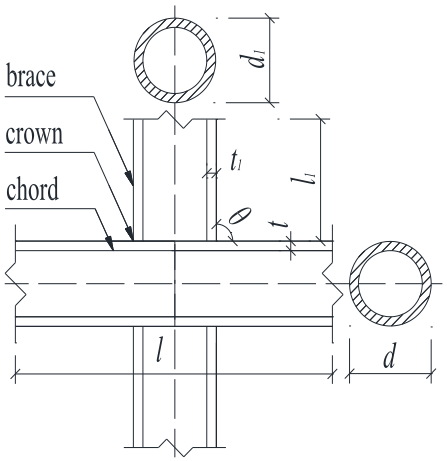

Fig. 4. Configuration and notations of CHS X-joints.

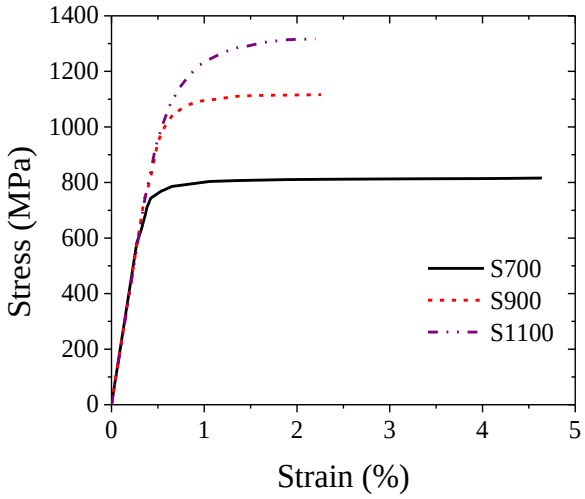

Fig. 5. Stress-strain curves of high strength steel (Ma et al. [22]).

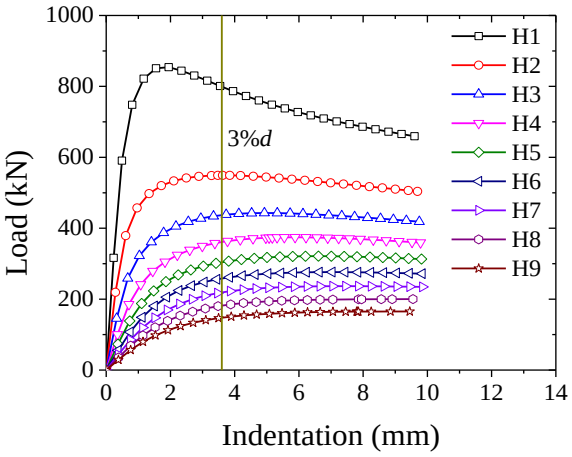

(a) Effect of β

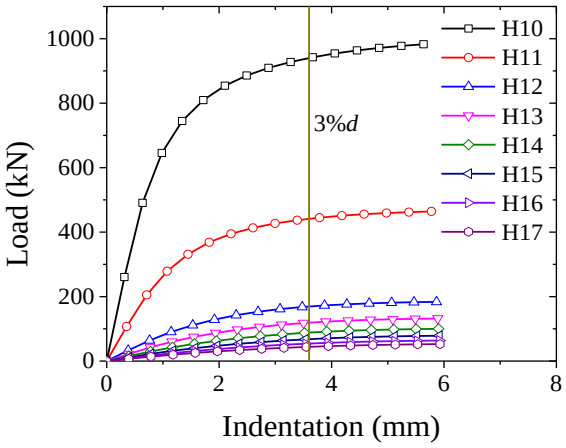

(b) Effect of 2γ

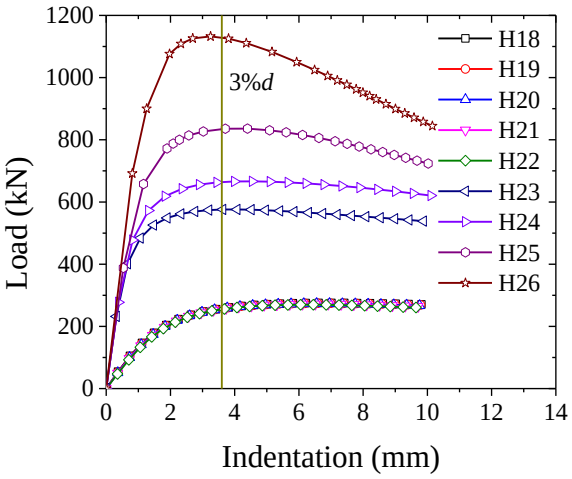

(c) Effect of θ and τ

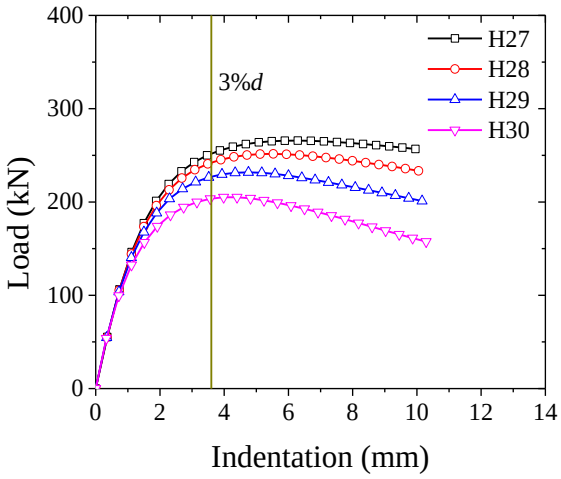

(d) Effect of n

Fig. 6. Load-indentation curves of CHS X-joints made of S700 steel.

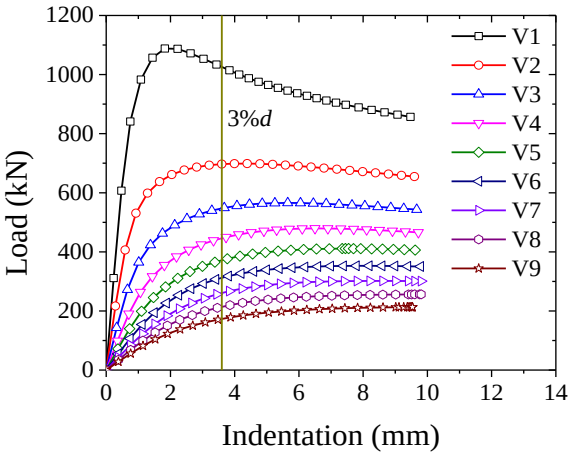

(a) Effect of β

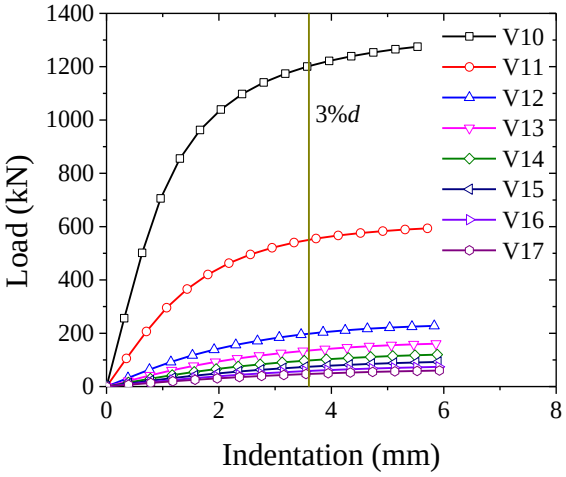

(b) Effect of 2γ

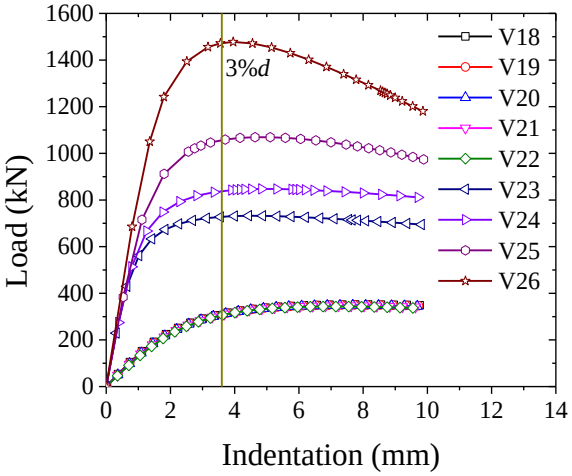

(c) Effect of θ and τ

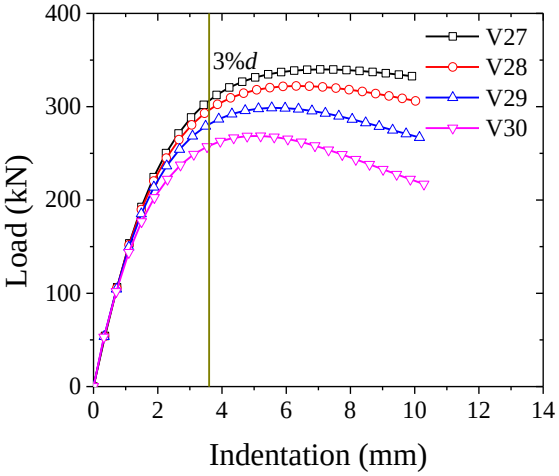

(d) Effect of n

Fig. 7. Load-indentation curves of CHS X-joints made of S900 steel.

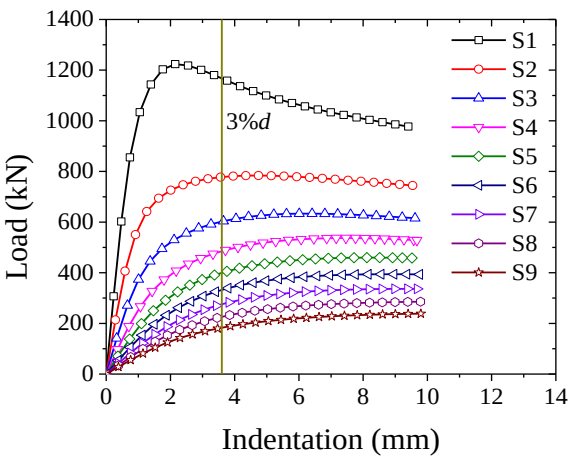

(a) Effect of β

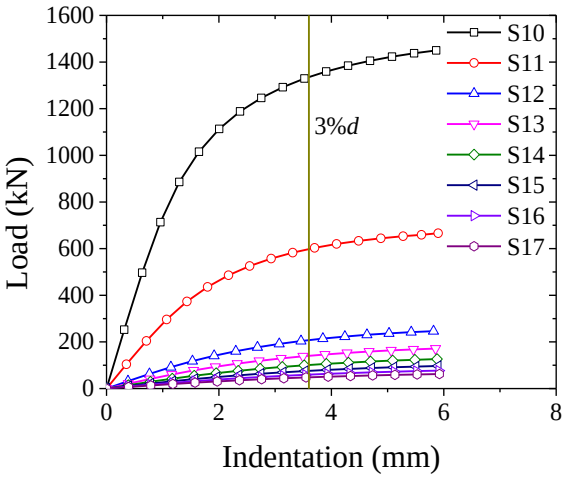

(b) Effect of 2γ

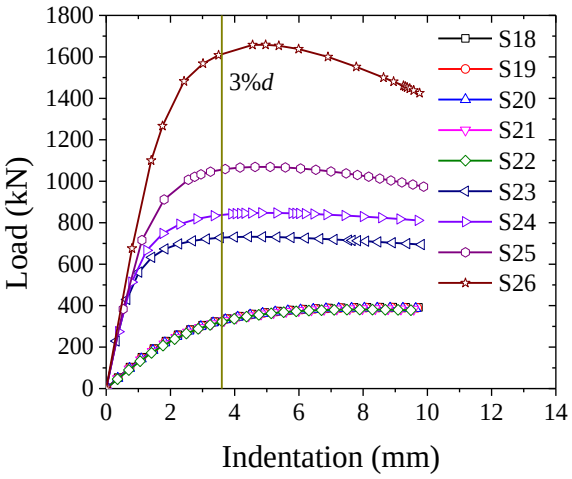

(c) Effect of θ and τ

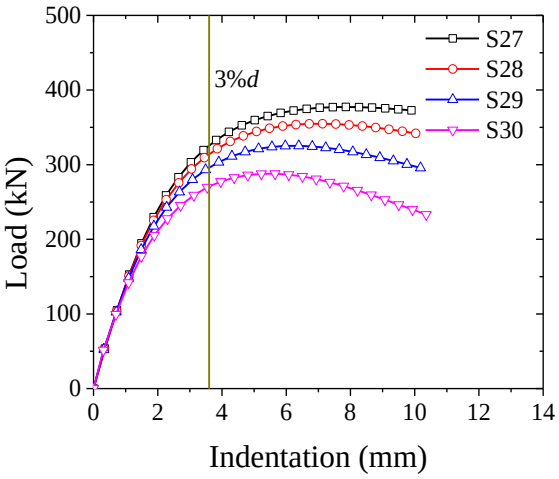

(d) Effect of n

Fig. 8. Load-indentation curves of CHS X-joints made of S1100 steel.

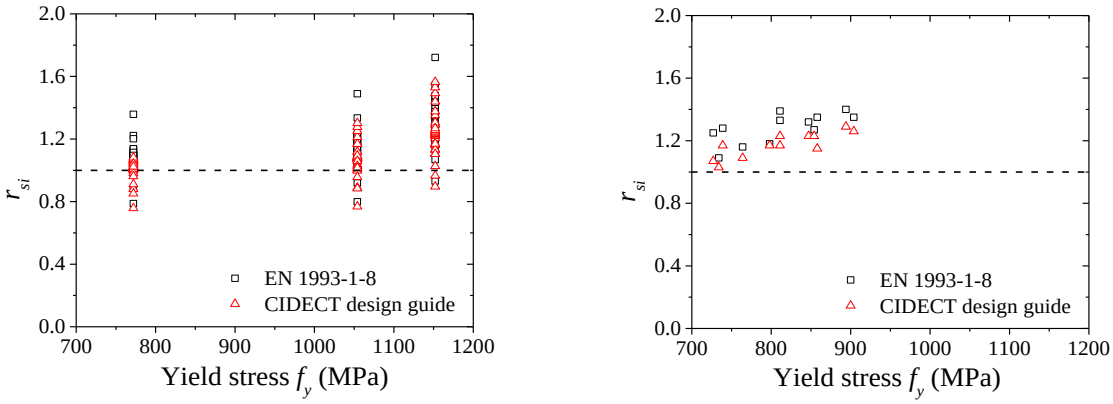

(a) Numerical results

(b) Test results

Fig. 9. Comparison of nominal strength predictions with numerical and test strengths.

Table 1

Specimens used for validating FE models.

Specimen	d(mm)	t(mm)	d_1(mm)	t_1(mm)	β	2γ	fy(MPa)	fu(MPa)
R32 [12]	324.7	14.8	177.9	8.4	0.55	21.94	734	802
R33 [12]	325.1	19.1	178.1	8.5	0.55	17.02	739	798
R47 [12]	324.8	20.3	178.0	8.5	0.55	16.00	376	575
R69 [12]	159.2	9.2	60.6	5.2	0.38	17.30	858	879
R71 [12]	193.8	10.1	139.7	7.2	0.72	19.19	854	900
R75 [12]	244.7	22.0	194.6	16.0	0.80	11.12	811	863
X90-650-0.75-16 [17]	400.0	25.0	300.0	15.0	0.75	16.00	806	938
X90-650-0.62-26 [17]	650.0	25.0	400.0	25.0	0.62	26.00	798	914

Table 2

Results of mesh convergence study on specimen R69.

Element type	Mesh size (mm)			N_{FE} / N_{Test}
	Joint zone	Outside joint zone	Weld	
Shell element	15	30	—	1.11
	10	20	—	1.07
	5	10	—	1.04
	3	6	—	1.04
Solid element	12	24	6	1.09
	10	20	5	1.08
	8	16	3	1.05
	6	10	2	1.05

Note: N_{Test} =519 kN.

Table 3

Comparison of joint strength.

Specimen	Element type	Mesh size (mm)			N_{FE} (kN)	N_{Test} (kN)	N_{FE} / N_{Test}
		Joint zone	Outside joint zone	Weld			
R32 [12]	Shell	10	20	—	1642	1774	0.93
R33 [12]	Shell	10	20	—	2620	2531	1.04
R47 [12]	Shell	10	20	—	1726	1598	1.08
R69 [12]	Shell	5	10	—	541	519	1.04
	Solid	8	16	3	547		1.05
R71 [12]	Shell	6	12	—	1124	1095	1.03
	Solid	10	20	4	1183		1.08
R75 [12]	Shell	8	16	—	5405	5298	1.02
	Solid	12	24	2	5279		1.00
X90-650-0.75-16 [17]	Shell	12	24	—	6750	6965	0.97
X90-650-0.62-26 [17]	Shell	20	40	—	5301	5612	0.94
Mean							1.02
COV							0.051

Table 4

Parameters for CHS X-joints made of S700, S900 and S1100 steel.

Joint number	d (mm)	t (mm)	d_1 (mm)	t_1 (mm)	θ (°)	n	τ	2γ	β
1	120	6.00	120	6.00	90	0	1.00	20.00	1.00
2	120	6.00	108	6.00	90	0	1.00	20.00	0.90
3	120	6.00	96	6.00	90	0	1.00	20.00	0.80
4	120	6.00	84	6.00	90	0	1.00	20.00	0.70
5	120	6.00	72	6.00	90	0	1.00	20.00	0.60
6	120	6.00	60	6.00	90	0	1.00	20.00	0.50
7	120	6.00	48	6.00	90	0	1.00	20.00	0.40
8	120	6.00	36	6.00	90	0	1.00	20.00	0.30
9	120	6.00	24	6.00	90	0	1.00	20.00	0.20
10	120	12.00	60	12.00	90	0	1.00	10.00	0.50
11	120	8.00	60	8.00	90	0	1.00	15.00	0.50
12	120	4.80	60	4.80	90	0	1.00	25.00	0.50
13	120	4.00	60	4.00	90	0	1.00	30.00	0.50
14	120	3.43	60	3.43	90	0	1.00	35.00	0.50
15	120	3.00	60	3.00	90	0	1.00	40.00	0.50
16	120	2.67	60	2.67	90	0	1.00	45.00	0.50
17	120	2.40	60	2.40	90	0	1.00	50.00	0.50
18	120	6.00	60	5.40	90	0	0.90	20.00	0.50
19	120	6.00	60	4.80	90	0	0.80	20.00	0.50
20	120	6.00	60	4.20	90	0	0.70	20.00	0.50
21	120	6.00	60	3.60	90	0	0.60	20.00	0.50
22	120	6.00	60	3.00	90	0	0.50	20.00	0.50
23	120	6.00	108	6.00	75	0	1.00	20.00	0.90
24	120	6.00	108	6.00	60	0	1.00	20.00	0.90
25	120	6.00	108	6.00	45	0	1.00	20.00	0.90
26	120	6.00	108	6.00	30	0	1.00	20.00	0.90
27	120	6.00	60	6.00	90	0.2	1.00	20.00	0.50
28	120	6.00	60	6.00	90	0.4	1.00	20.00	0.50
29	120	6.00	60	6.00	90	0.6	1.00	20.00	0.50
30	120	6.00	60	6.00	90	0.8	1.00	20.00	0.50

Table 5

Material parameters for high strength steel (Ma et al. [22]).

Steel grade	E (GPa)	$\sigma_{0.01}$ (MPa)	$\sigma_{0.2}$ (MPa)	σ_u (MPa)	ε_u (%)
S700	214	582	772	816	4.64
S900	210	736	1054	1116	2.26
S1100	207	727	1152	1317	2.20

Table 6

Comparison of nominal strengths of CHS X-joints made of S700 steel with numerical strengths.

Specimen	β	2γ	n	τ	θ (°)	N_{FE} (kN)	Comparison	
							N_{EC}/N_{FE}	N_{CIDECT}/N_{FE}
H1	1.00	20.00	0	1.00	90	854.0	1.04	0.88
H2	0.90	20.00	0	1.00	90	549.1	1.13	1.06
H3	0.80	20.00	0	1.00	90	436.9	1.09	1.06
H4	0.70	20.00	0	1.00	90	361.0	1.07	1.04
H5	0.60	20.00	0	1.00	90	304.0	1.08	1.02
H6	0.50	20.00	0	1.00	90	258.2	1.09	1.01
H7	0.40	20.00	0	1.00	90	218.9	1.14	1.00
H8	0.30	20.00	0	1.00	90	181.6	1.22	1.02
H9	0.20	20.00	0	1.00	90	147.6	1.36	1.07
H10	0.50	10.00	0	1.00	90	940.0	1.20	1.00
H11	0.50	15.00	0	1.00	90	441.1	1.14	1.01
H12	0.50	25.00	0	1.00	90	169.3	1.07	1.02
H13	0.50	30.00	0	1.00	90	119.1	1.05	1.03
H14	0.50	35.00	0	1.00	90	88.3	1.04	1.05
H15	0.50	40.00	0	1.00	90	67.9	1.04	1.06
H16	0.50	45.00	0	1.00	90	54.2	1.03	1.07
H17	0.50	50.00	0	1.00	90	44.2	1.02	1.08
H18	0.50	20.00	0	0.90	90	257.8	1.10	1.01
H19	0.50	20.00	0	0.80	90	257.4	1.10	1.01
H20	0.50	20.00	0	0.70	90	256.8	1.10	1.01
H21	0.50	20.00	0	0.60	90	256.0	1.10	1.02
H22	0.50	20.00	0	0.50	90	254.7	1.11	1.02
H23	0.90	20.00	0	1.00	75	575.7	1.11	1.04
H24	0.90	20.00	0	1.00	60	663.9	1.08	1.01
H25	0.90	20.00	0	1.00	45	834.2	1.05	0.98
H26	0.90	20.00	0	1.00	30	1132.3	1.09	1.02
H27	0.50	20.00	0.2	1.00	90	251.7	1.04	0.96
H28	0.50	20.00	0.4	1.00	90	242.1	0.97	0.91
H29	0.50	20.00	0.6	1.00	90	227.0	0.89	0.85
H30	0.50	20.00	0.8	1.00	90	203.6	0.79	0.76
Mean							1.08	1.00
COV							0.09	0.07

Table 7

Comparison of nominal strengths of CHS X-joints made of S900 steel with numerical strengths.

Specimen	β	2γ	n	τ	θ (°)	N_{FE} (kN)	Comparison	
							N_{EC} / N_{FE}	N_{CIDECT} / N_{FE}
V1	1.00	20.00	0	1.00	90	1088.1	1.04	0.89
V2	0.90	20.00	0	1.00	90	697.0	1.14	1.07
V3	0.80	20.00	0	1.00	90	547.2	1.12	1.08
V4	0.70	20.00	0	1.00	90	445.8	1.12	1.09
V5	0.60	20.00	0	1.00	90	371.6	1.13	1.08
V6	0.50	20.00	0	1.00	90	312.2	1.16	1.07
V7	0.40	20.00	0	1.00	90	260.7	1.23	1.08
V8	0.30	20.00	0	1.00	90	213.8	1.33	1.12
V9	0.20	20.00	0	1.00	90	173.1	1.49	1.17
V10	0.50	10.00	0	1.00	90	1202.0	1.21	1.00
V11	0.50	15.00	0	1.00	90	550.3	1.17	1.04
V12	0.50	25.00	0	1.00	90	198.0	1.17	1.12
V13	0.50	30.00	0	1.00	90	135.4	1.19	1.17
V14	0.50	35.00	0	1.00	90	98.0	1.21	1.21
V15	0.50	40.00	0	1.00	90	74.2	1.22	1.25
V16	0.50	45.00	0	1.00	90	58.5	1.23	1.28
V17	0.50	50.00	0	1.00	90	47.2	1.23	1.30
V18	0.50	20.00	0	0.90	90	311.5	1.17	1.08
V19	0.50	20.00	0	0.80	90	310.6	1.17	1.08
V20	0.50	20.00	0	0.70	90	309.4	1.17	1.08
V21	0.50	20.00	0	0.60	90	308.0	1.18	1.09
V22	0.50	20.00	0	0.50	90	306.0	1.19	1.09
V23	0.90	20.00	0	1.00	75	727.9	1.13	1.06
V24	0.90	20.00	0	1.00	60	837.3	1.10	1.03
V25	0.90	20.00	0	1.00	45	1056.2	1.07	1.00
V26	0.90	20.00	0	1.00	30	1472.4	1.08	1.01
V27	0.50	20.00	0.2	1.00	90	306.4	1.10	1.02
V28	0.50	20.00	0.4	1.00	90	296.4	1.02	0.96
V29	0.50	20.00	0.6	1.00	90	281.2	0.92	0.88
V30	0.50	20.00	0.8	1.00	90	258.1	0.80	0.77
Mean							1.15	1.07
COV							0.10	0.10

Table 8

Comparison of nominal strengths of CHS X-joints made of S1100 steel with numerical strengths.

Specimen	β	2γ	n	τ	θ (°)	N_{FE} (kN)	Comparison	
							N_{EC}/N_{FE}	N_{CIDECT}/N_{FE}
S1	1.00	20.00	0	1.00	90	1223.7	1.14	0.97
S2	0.90	20.00	0	1.00	90	777.7	1.25	1.17
S3	0.80	20.00	0	1.00	90	602.3	1.25	1.20
S4	0.70	20.00	0	1.00	90	485.0	1.26	1.22
S5	0.60	20.00	0	1.00	90	399.7	1.29	1.22
S6	0.50	20.00	0	1.00	90	332.2	1.34	1.23
S7	0.40	20.00	0	1.00	90	275.5	1.42	1.25
S8	0.30	20.00	0	1.00	90	225.8	1.54	1.29
S9	0.20	20.00	0	1.00	90	183.0	1.72	1.35
S10	0.50	10.00	0	1.00	90	1335.3	1.33	1.10
S11	0.50	15.00	0	1.00	90	598.0	1.32	1.17
S12	0.50	25.00	0	1.00	90	207.4	1.37	1.31
S13	0.50	30.00	0	1.00	90	140.4	1.40	1.38
S14	0.50	35.00	0	1.00	90	101.0	1.43	1.44
S15	0.50	40.00	0	1.00	90	76.0	1.46	1.49
S16	0.50	45.00	0	1.00	90	59.7	1.47	1.53
S17	0.50	50.00	0	1.00	90	48.0	1.48	1.56
S18	0.50	20.00	0	0.90	90	331.0	1.34	1.24
S19	0.50	20.00	0	0.80	90	329.6	1.35	1.24
S20	0.50	20.00	0	0.70	90	327.8	1.35	1.25
S21	0.50	20.00	0	0.60	90	325.5	1.36	1.26
S22	0.50	20.00	0	0.50	90	322.6	1.38	1.27
S23	0.90	20.00	0	1.00	75	810.8	1.24	1.16
S24	0.90	20.00	0	1.00	60	930.0	1.21	1.13
S25	0.90	20.00	0	1.00	45	1165.8	1.18	1.10
S26	0.90	20.00	0	1.00	30	1607.9	1.21	1.13
S27	0.50	20.00	0.2	1.00	90	325.5	1.27	1.17
S28	0.50	20.00	0.4	1.00	90	313.9	1.18	1.10
S29	0.50	20.00	0.6	1.00	90	295.9	1.07	1.03
S30	0.50	20.00	0.8	1.00	90	270.7	0.93	0.90
Mean							1.32	1.23
COV							0.11	0.12

Table 9

Ranges of geometric parameters.

Geometric parameter	$\beta=d_1/t$	$2\gamma=d/t$	$\tau=t_1/t$	θ (°)
EN 1993-1-8 [1]	[0.2-1.0]	[10-50]	—	[30-90]
CIDECT design guide [3]	[0.2-1.0]	≤40	≤1.0	[30-90]
Numerical analysis	[0.2-1.0]	[10-50]	[0.5-1.0]	[30-90]

Table 10

Comparison of nominal strengths of CHS X-joints with test strengths.

Specimen	β	2γ	Steel grade	f_y (MPa)	f_u (MPa)	N_{Test} (kN)	Comparison	
							N_{EC}/N_{Test}	N_{CIDECT}/N_{Test}
R32 [12]	0.55	21.94	S690	734	802	1774	1.09	1.03
R33 [12]	0.55	17.02	S690	739	798	2531	1.28	1.17
R42 [12]	1.00	21.45	S690	727	793	1399	1.25	1.07
R68 [12]	0.62	17.24	S770	904	946	314	1.35	1.26
R69 [12]	0.38	17.30	S770	858	879	519	1.35	1.15
R70 [12]	0.77	15.18	S770	847	892	968	1.32	1.23
R71 [12]	0.72	19.19	S770	854	900	1095	1.27	1.23
R72 [12]	0.53	18.92	S770	894	937	1868	1.40	1.29
R74 [12]	0.65	11.12	S770	811	863	4143	1.33	1.17
R75 [12]	0.80	11.12	S770	811	863	5298	1.39	1.23
X90-650-0.75-16 [17]	0.75	16.00	HSA800	764	938	6965	1.16	1.09
X90-650-0.62-26 [17]	0.62	26.00	HSA800	798	914	5612	1.18	1.17
Mean							1.28	1.17
COV							0.08	0.07

Note: The nominal yield stress and ultimate stress of HSA800 steel are 650 and 800 MPa, respectively.

Table 11

Statistical analysis for the strength ratio.

Comparison	Mean	COV	*e*	s
EN 1993-1-8 [1]	1.19	0.13	20.7%	24.9%
CIDECT design guide [3]	1.11	0.13	13.5%	18.2%